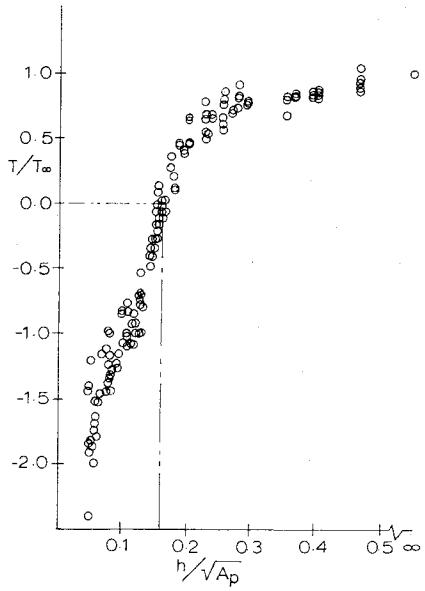

Fig. 2 Nondimensionalized thrust vs height.

ground effect region was less than that out of ground effect as is expected with this configuration. The loss in this net positive thrust was due to the high-velocity flow parallel to the surfaces. This flow creates a low static pressure on the lower vehicle surface. Since ambient pressure is acting on the upper vehicle surface a pressure differential exists across the vehicle surface. The integral of this pressure differential across the entire surface was the ground effect force and of course acted in a direction opposite to the thrust produced by the flow through the nozzle. When the two forces are equal and opposite the vehicle experiences no net force. The height at which this occurs has been called the critical height. For separation less than this, the ground effect force is greater than the thrust due to mass flow and the net force on the vehicle is toward the ground plane. The ground effect force actually became several times the magnitude of the original thrust out of ground effect for separations smaller than the critical height. It was found that, of all the parameters tested, only the planform area (which included the nozzle area) had an effect on the value of the critical height. Once at the critical height for a certain planform, a change in mass flow, nozzle size, nozzle geometry, or aspect ratio (less than three) had no effect in changing the net thrust from its zero value. For a given planform area, at any pressure ratio the flow created a ground effect force exactly equal to the thrust due to mass flow at the same height. This is the critical height phenomenon. Plots were made of the ratio of thrust at any height divided by the thrust out of ground effect, T/T_∞, vs the height divided by the square root of the planform area (Fig. 2). In each case the critical value of $h/(A_p)^{1/2}$ where T/T_∞ was zero was about 0.16. This is very close to $\frac{1}{2\pi}$. Since only circular and elliptical shapes were used for the vehicle surface, a comparison of the data obtained by Spreeman and Sherman[1] for square and rectangular shapes was made. Again the critical height had the same value when nondimensionalized with respect to the square root of the planform area.

The range of values tested included: plenum chamber pressures of from 5 to 20 psi above ambient; planform areas of from 4.43 to 95.1 in.^{2}; planform-to-nozzle area ratios of from 21.6 to 485; aspect ratios less than three; nozzle minimum areas of 0.106 and 0.785 in.^{2}; and nozzle divergence of 0 and 24° total angle.

Concluding Remarks

An experimental investigation has led to the discovery of the critical height phenomenon. A cold-flow test procedure found that, of the parameters tested and within the limits tested, only the vehicle surface area had an effect on the value of the critical height, and therefore that nondimensionalizing the critical height with respect to the area gave the same value for all configurations. This value was found to be given very closely by $\frac{1}{2\pi}$.

References

[1] Spreeman, K. P. and Sherman, I. R., "Effects of Ground Proximity on the Thrust of a Simple Downward-Directed Jet Beneath a Flat Surface," TN 4407, 1958, NACA.

[2] von Glahn, Uwe H., "Exploratory Study of Ground Proximity Effects on Thrust of Annular and Circular Nozzles," TN 3982, 1957, NACA.

Skin-Friction Measurement at Supersonic Speeds

F. K. Owen* and B. J. Bellhouse†
University of Oxford, Oxford, England

Nomenclature

i = hot film current
k = thermal conductivity
L = streamwise length of heated film
q = mean heat transfer per unit area
R = hot film operating resistance
ΔT = temperature difference between hot film and local recovery temperature
μ = viscosity
ρ = density
σ = Prandtl number
τ = shear stress

Subscript

w = wall condition

Theoretical Considerations

It has been shown that the wall shearing stress of a laminar or turbulent boundary layer in incompressible flow can be determined from heat-transfer measurements at the surface (Ref. 1). In this case, it is possible to restrict the temperature difference ΔT to values small enough to neglect variations of μ, ρ, and k. However, in order to extend the previous equations to high-speed flow, variations of fluid properties due to temperature variations in the boundary layer must be considered.

For a small heated element the thermal boundary-layer thickness is much less than the velocity boundary-layer thickness, so when solving the energy integral equation the velocity may be approximated by

$$u = (\tau_w/\mu)y + (1/2\mu)(dp/dx)y^2 \qquad (1)$$

Thus, it has been shown in Refs. 1 and 2 that in zero-pressure-gradient, incompressible, laminar flow the heat transfer from a hot film is related to the mass flow-rate near the surface by the equation

$$Nu = (q_w L/k\Delta T)\alpha(\rho\tau/\mu^2)^{1/3}(\sigma L^2)^{1/3} \qquad (2)$$

Liepmann and Skinner[2] extended this analysis to turbulent boundary layers under the assumption that the temperature field due to the heated film constituted a thermal boundary layer that was contained entirely within the laminar sub-

Received January 29, 1970; revision received April 6, 1970.

* Research Student; now Postdoctoral Research Associate, NASA-Ames Research Center, Moffett Field, Calif.

† Lecturer, Department of Engineering Science.

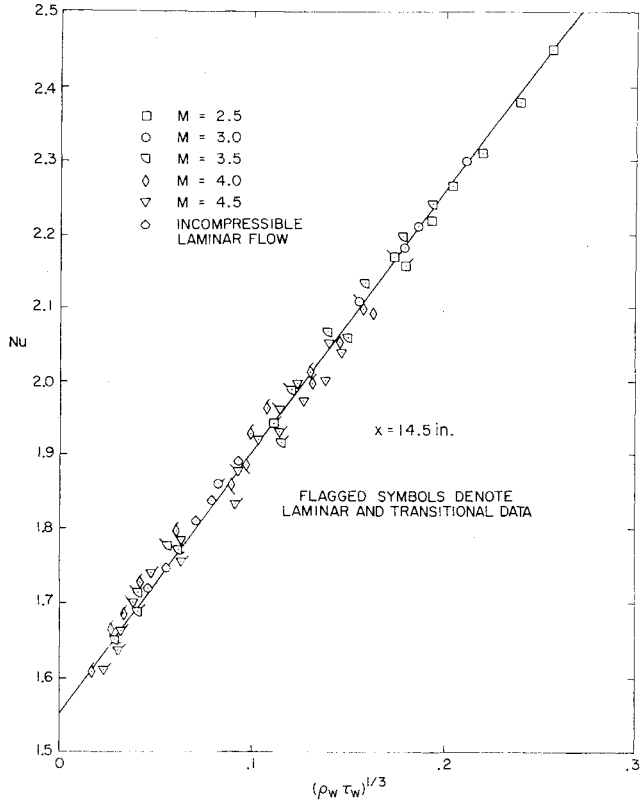

Fig. 1 Thin film gage calibration in compressible, laminar and turbulent boundary layers.

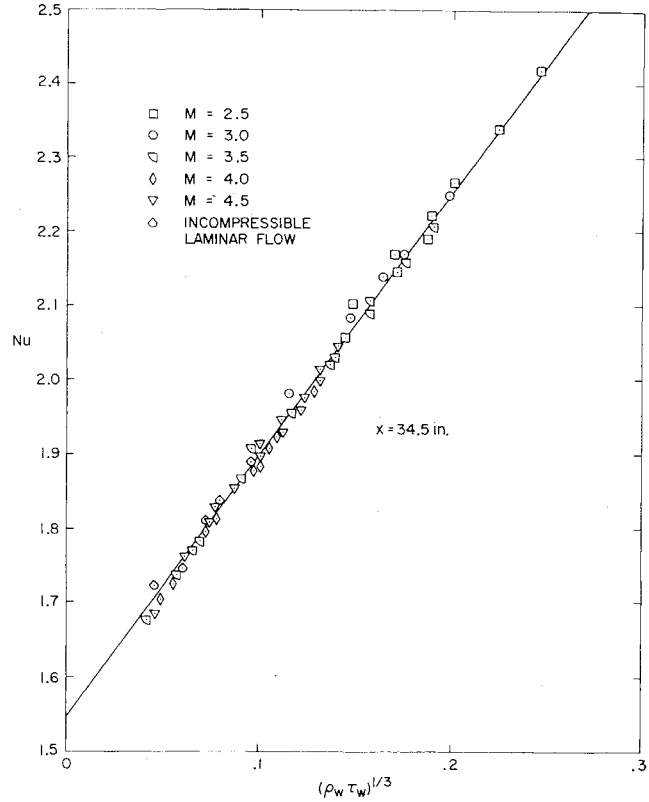

Fig. 2 Thin film gage calibration in compressible, turbulent boundary layers.

layer in which turbulent fluctuations were supposed to be negligible.

Since the thermal boundary layer produced by a heated film is confined to a region close to the wall, in compressible flow, it might be expected that the average fluid properties across the thermal boundary layer produced by the heated film would be close to the wall values as proposed by Bellhouse and Schultz.[3] So if the specific heat and the Prandtl number are taken to be constant, Eq. 2 may be written

$$Nu = (q_w L/k\Delta T)\alpha(\rho_w \tau_w/\mu_w)^{1/3} L^{2/3} \tag{3}$$

For a heated film

$$q_w L/k\Delta T = A(i^2 R/\Delta T) + B \tag{4}$$

where B represents the heat loss to the substrate. So for a given probe at constant wall temperature, Eq. 3 reduces to

$$i^2 R/\Delta T = C(\rho_w \tau_w)^{1/3} + D \tag{5}$$

where C and D are probe constants.

Discussion

The heat-transfer measurements were made with a platinum thin-film gage deposited on a pyrex glass substrate. The film was maintained at constant temperature by a feedback bridge. The data were obtained on an adiabatic flat plate with a bevel angle of 10° and leading edge thickness 0.010 in. at unit Reynolds numbers up to 14×10^6 per ft at $M = 2.5$ and 10×10^6 per ft at $M = 4.5$.

The heated element was mounted in a metal insert flush with the model surface at distances of 14.5 and 34.5 in. from the leading edge. The insert was also instrumented with a second thin film for surface temperature measurement and three static pressure holes for surface pressure measurement. The local skin friction was measured by a floating element balance at the two hot-film probe positions.

The tunnel total temperature was varied with Mach number in an attempt to maintain a constant plate temperature. However, there was some variation of equilibrium temperature. At the forward position the temperature tended to be higher and the scatter greater. This is due to conduction from the higher temperatures in the stagnation and compression region on the under surface of the model, and to changes in the recovery factor caused by boundary-layer transition at the 14.5-in. probe position (see Ref. 4).

The thin-film data at the two positions are shown in Figs. 1 and 2 where it can be seen that the calibration is independent of Mach number, thus confirming the results in Ref. 3 for compressible turbulent boundary layers. However, Fig. 1 also shows that there is a unique calibration for laminar and turbulent flow at supersonic speeds and that the laminar incompressible points, obtained on a flat plate in a low-speed wind tunnel, fall close to the supersonic calibration. The reason there are no significant differences between the compressible laminar and turbulent calibrations is probably that the thickening of the laminar sublayer (the region where molecular viscosity predominates) at supersonic speeds reduces the fluctuations in the wall region so that turbulent heat and momentum transfer are negligible. It is these fluctuations that change the effective fluid properties close to the wall in incompressible flow and are responsible for differences in calibrations at subsonic speeds.[1]

Also shown is a least squares fit to the data. Assuming that the skin-friction values given by the floating element are correct, the probable error in skin friction predicted by the thin film at the 14.5-in. position is 13% and at the 34.5-in. position 5%. We conclude that calibrations made in laminar boundary layers at subsonic speeds can be extended to laminar and turbulent compressible flow.

References

[1] Bellhouse, B. J. and Schultz, D. L., "Determination of Mean and Dynamic Skin Friction, Separation and Transition in Low-Speed Flow with a Thin Film Heated Element," *Journal of Fluid Mechanics*, Vol. 24, Pt. 2, 1966, p. 379.

[2] Liepmann, H. W. and Skinner, G. T., "Shearing Stress Measurements by Use of Heated Element," TN 3268, 1954, NACA.
[3] Bellhouse, B. J. and Schultz, D. L., "The Measurement of Skin Friction in Supersonic Flow by Means of Heated Thin Film Gauges," R and M 3490, 1968, Aeronautical Research Council.
[4] Owen, F. K., "Transition Experiments on a Flat Plate at Subsonic and Supersonic Speeds," *AIAA Journal*, Vol. 8, No. 3, March 1970, pp. 518–523.

Radiant Heat Transfer at the Vertex of Adjoint Plates

MAURICE L. RASMUSSEN*
AND
MARTIN C. JISCHKE†
University of Oklahoma, Norman, Okla.

Introduction

THE Fredholm integral equations of the second kind that govern radiant heat transfer do not lend themselves to analytical treatment. As a result there are few exact solutions. Moreover, when these equations are singular, certain difficulties are encountered in obtaining numerical solutions. A good example is that of radiant heat transfer for adjoint plates, which was first studied by Sparrow et al.[1] and more recently by Love and Turner.[2] Because the governing integral equation is singular at the vertex of the adjoint plates, the numerical solutions encounter convergence difficulties in this region. It appears, moreover, that these authors could not obtain satisfactory convergence when the angle between the adjoint plates was small. This note is concerned with the analytical treatment at the vertex, which is of some theoretical as well as practical interest. The exact value of the heat transfer at the vertex is obtained together with the asymptotic behavior near the vertex.

Heat Transfer at the Vertex

The adjoint-plate configuration is shown in Fig. 1. The upper and lower plates have the same length, temperature, and surface properties (grey and diffuse), and they are separated by a vacuum. If the nondimensional distance and radiosity are denoted by $X = x/L$ and $\beta(X) = R(X)/\epsilon\sigma T^4$, the governing equation for $\beta(X)$ appears as[1,2]

$$\beta(X) = 1 + \lambda \int_0^1 \beta(Y)K(X,Y)dY \tag{1}$$

where

$$\lambda \equiv \tfrac{1}{2}\rho \sin^2\theta \tag{2}$$

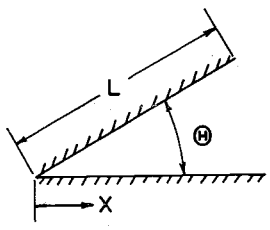

Fig. 1 Adjoint-plate configuration.

Received February 6, 1970. A number of valuable discussions of this problem with T. Love are gratefully acknowledged.
* Associate Professor, Aerospace and Mechanical Engineering. Member AIAA.
† Assistant Professor, Aerospace and Mechanical Engineering. Member AIAA.

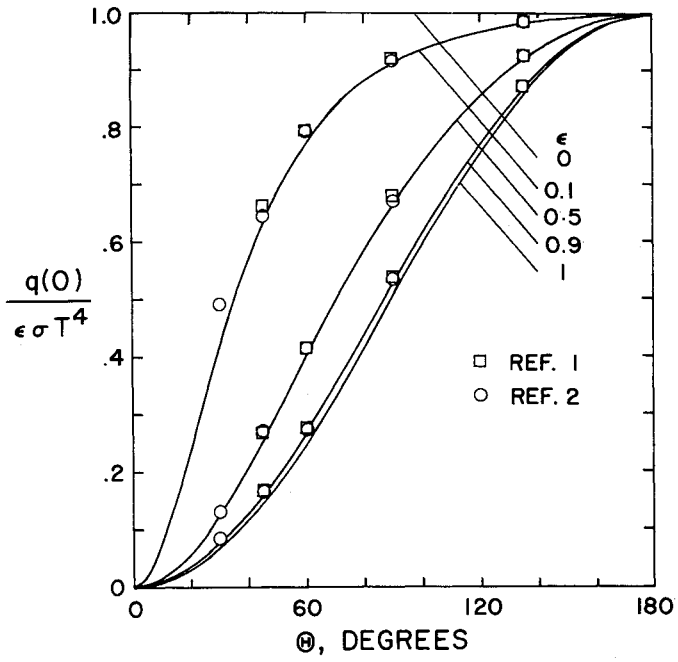

Fig. 2 Heat transfer at vertex.

$$K(X,Y) = XY[X^2 - 2XY\cos\theta + Y^2]^{-3/2} \tag{3}$$

and $\rho = (1 - \epsilon)$ is the reflectance.

Equation (1) can be written alternatively by means of the substitution $Y = Xu$;

$$\beta(X) = 1 + \lambda \int_0^{1/X} \beta(Xu)K(1,u)du \tag{4}$$

The radiosity at the vertex is determined by setting $X = 0$ in Eq. (4). We obtain

$$\beta(0) = 1 + \lambda\beta(0) \int_0^{\infty} K(1,u)du \tag{5}$$

After evaluating the integral in Eq. (5) by means of standard integral tables, we solve for $\beta(0)$ and obtain

$$\beta(0) = [1 - \rho\cos^2(\theta/2)]^{-1} \tag{6}$$

This is the exact value. The heat transfer is determined from the radiosity[1,2] and is found to be

$$\frac{q(0)}{\epsilon\sigma T^4} = \frac{1 - \epsilon\beta(0)}{\rho} = \frac{\sin^2(\theta/2)}{1 - \rho\cos^2(\theta/2)} \tag{7}$$

Equation (7) is plotted in Fig. 2 for various values of the emittance $\epsilon = (1 - \rho)$. Also shown are the numerical values obtained by Sparrow et al.[1] and Love and Turner.[2] The numerical values are seen to fall slightly above the exact values for the smaller values of θ and ϵ. This discrepancy arises because of the singular behavior of Eq. (1) at $X = 0$, which causes loss of accuracy in the numerical solution in this region. An asymptotic investigation reveals the nonanalytic behavior of the solution near $X = 0$.

Asymptotic Behavior

Preliminary investigation of the solution of Eq. (1) by means of the Neumann series[3] leads to the assumed behavior

$$\beta(X) \sim \beta_0 + \beta_1 X^{1-\alpha},\ X \to 0,\ 0 < \alpha < 1 \tag{8}$$

The constants β_0, β_1, and α are to be determined by substituting Eq. (8) into Eq. (4) and collecting like powers of X asymptotically as $X \to 0$. This procedure yields

$$\beta_0 + \beta_1 X^{1-\alpha} = (1 + \lambda\beta_0 b) - \lambda[\beta_0 + (\beta_1/\alpha)]X + \lambda\beta_1 Q(\alpha,\theta)X^{1-\alpha} + 0(X^2),\ X \to 0 \tag{9}$$